Effects of mode coupling on the admittance of an AT-cut quartz thickness-shear resonator*

He Hui-Jing(何慧晶)[a], Yang Jia-Shi(杨嘉实)[a]†, Zhang Wei-Ping(张卫平)[b], and Wang Ji(王 骥)[c]

[a] *Department of Mechanical and Materials Engineering, University of Nebraska-Lincoln, Lincoln, NE* 68588-0526, *USA*
[b] 1785 *Pebblewood Lane, Hoffman Estates, IL* 60195, *USA*
[c] *Piezoelectric Device Laboratory, School of Mechanical Engineering and Mechanics, Ningbo University, Ningbo* 315211, *China*

(Received 23 June 2012; revised manuscript received 9 September 2012)

We study the effects of couplings to flexure and face-shear modes on the admittance of an AT-cut quartz plate thickness-shear mode resonator. Mindlin's two-dimensional equations for piezoelectric plates are employed. Electrically forced vibration solutions are obtained for three cases: pure thickness-shear mode alone; two coupled modes of thickness shear and flexure; and three coupled modes of thickness shear, flexure, and face shear. Admittance is calculated and its dependence on the driving frequency and the length/thickness ratio of the resonator is examined. Results show that near the thickness-shear resonance, admittance assumes maxima, and that for certain values of the length/thickness ratio, the coupling to flexure causes severe admittance drops, while the coupling to the face-shear mode causes additional admittance changes that were previously unknown and hence are not considered in current resonator design practice.

Keywords: quartz, plate, resonance, resonator

PACS: 77.65.Fs, 77.65.−j **DOI:** 10.1088/1674-1056/22/4/047702

1. Introduction

Piezoelectric crystals are widely used to make acoustic wave resonators as frequency standards for time-keeping, frequency operation, telecommunications, and sensing. In these applications crystal resonators operate as elements of electrical circuits for alternating currents called oscillators. Two basic properties of a crystal resonator, its resonant frequency and its electrical admittance, are of primary interest for complete circuit analyses of oscillators. There exist extensive theoretical results on crystal resonators using the equations of anisotropic elasticity or piezoelectricity, e.g., Refs. [1]–[8]. More references can be found in a review article.[9] These analyses were overwhelmingly for resonator-free vibration frequency analysis. The admittance of a resonator, which can only be obtained from an electrically forced vibration analysis, was studied less often. Limited by the computational capability available, early forced vibration analyses had limited numerical results, e.g., Refs. [10]–[13]. Recently, there has been growing interest in the computation of resonator admittance, e.g., Refs. [14]–[21]. However, usually only the dependence of the admittance on the driving frequency of the applied voltage was examined. The dependence of the admittance on the plate aspect ratio (length/thickness) and the related admittance drop due to mode couplings was rarely studied, for which limited numerical results can be found in Refs. [14] and [15] for coupled thickness-shear and flexural motions of a resonator.

From the frequency spectra[1] obtained in resonator-free vibration frequency analysis, it can be expected that as the aspect ratio of a resonator changes, for certain discrete values of the aspect ratio, the operating thickness-shear mode of the resonator becomes coupled to other unwanted modes and the resonator admittance dips. For the case of coupled thickness shear and flexure, this was confirmed by the limited numerical results in Refs. [14] and [15]. However, for a resonator with a properly designed aspect ratio so that coupling to flexure is avoided, sometimes unexpected and sudden changes of admittance still occur. It has been suspected that maybe the coupling to some other unwanted modes is involved, but this has not been confirmed theoretically, and it is not clear specifically which unwanted mode is causing the additional admittance drop.

It is known[3,13] that, in the frequency range of interest from zero to slightly above the fundamental thickness-shear frequency, the operating thickness-shear mode is also coupled to the face-shear mode[3,13] in addition to flexure. The coupling to face shear is through the relatively small elastic constant c_{56} and therefore is usually neglected. However, since the face-shear mode directly contributes to the charge and current through the piezoelectric constant e_{25} which is of the same order of magnitude as the main piezoelectric constant e_{26} in the most widely used AT-cut quartz resonators, the face-shear mode is expected to have some effect on resonator admittance. At present little is known about this effect, either qualitatively or quantitatively. In particular, we suspect that the face-shear

*Project supported in part by the National Natural Science Foundation of China (Grant Nos. 10932004, 11072116, and 10772087) and the Doctoral Program Fund of Ministry of Education of China (Grant No. 20093305110003/JW). Additional Funds were from the Sir Y. K. Pao Chair Professorship, the K. C. Wong Magna Fund through Ningbo University, and the K. C. Wong Education Foundation in Hong Kong. The project also supported in part by the US Army Research Laboratory/US Army Research Office (Grant No. W911NF-10-1-0293).

†Corresponding author. E-mail: jyang1@unl.edu

© 2013 Chinese Physical Society and IOP Publishing Ltd

mode may be related to the so far unexplained additional admittance drops when coupling to flexure is already excluded.

Therefore, in this paper, we study the effect of resonator aspect ratio on admittance through an electrically forced vibration analysis in a manner more general and systematic than Refs. [14] and [15]. The main difference from Refs. [14] and [15] is that the face-shear mode is included in the present analysis. Due to material anisotropy and piezoelectric coupling, theoretical analyses of crystal resonators usually present considerable mathematical challenges. To simplify the analysis of plate resonators, in a series of papers (Refs. [10], [11], and [22]–[24]), Mindlin and his coworkers developed and refined the two-dimensional equations for motions of piezoelectric plates which have been widely used for both theoretical and numerical analyses of crystal resonators, and are also used in the present paper.

2. Equations for piezoelectric plates

Consider a thin piezoelectric plate with thickness $2b$ as shown in Fig. 1 along with its coordinate system. The two major surfaces of the plate at $x_2 = \pm b$ are fully electroded. We assume thin electrodes whose mechanical effects like inertia and stiffness are negligible. We study vibrations independent of x_3 which are called straight-crested wave (modes).[1,2,6,7,10]

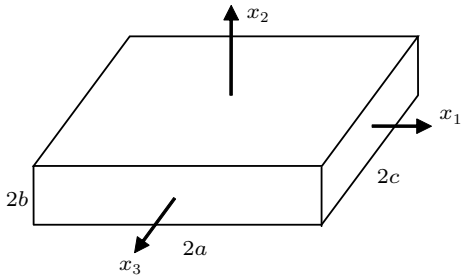


Fig. 1. An AT-cut quartz plate and coordinate system.

In the frequency range of interest, the three relevant waves are governed by Mindlin's first-order plate theory[23,25]

$$\begin{aligned} T^{(0)}_{13,1} &= 2b\rho\ddot{u}^{(0)}_3, \\ T^{(0)}_{12,1} &= 2b\rho\ddot{u}^{(0)}_2, \\ T^{(1)}_{11,1} - T^{(0)}_{21} &= \frac{2b^3}{3}\rho\ddot{u}^{(1)}_1, \end{aligned} \tag{1}$$

where $u^{(0)}_3(x_1,t)$ is the plate face-shear displacement, $u^{(0)}_2(x_1,t)$ is the flexural displacement, and $u^{(1)}_1(x_1,t)$ is the thickness-shear displacement. For crystals of monoclinic symmetry which include the most widely used AT-cut quartz as a special case, the plate resultants $T^{(0)}_{13}$, $T^{(0)}_{12}$, and $T^{(1)}_{11}$ describing the bending moment and various shear forces are given by the following plate constitutive relations:[23,25]

$$\begin{aligned} T^{(0)}_{13} &= \int_{-b}^{b} T_{13}\,\mathrm{d}x_2 = 2b(c_{55}S^{(0)}_5 + \kappa_1 c_{56}S^{(0)}_6 - e_{25}E^{(0)}_2), \\ T^{(0)}_{12} &= \int_{-b}^{b} T_{12}\,\mathrm{d}x_2 = 2b(\kappa_1 c_{56}S^{(0)}_5 + \kappa_1^2 c_{66}S^{(0)}_6 - \kappa_1 e_{26}E^{(0)}_2), \\ T^{(1)}_{11} &= \int_{-b}^{b} x_2 T_{11}\,\mathrm{d}x_2 = \frac{2b^3}{3}(\gamma_{11}S^{(1)}_1 - \psi_{11}E^{(1)}_1), \end{aligned} \tag{2}$$

where c_{pq}, e_{kp}, and ε_{kl} are the usual elastic stiffness, piezoelectric constants, and dielectric constants. The plate strains $S^{(0)}_5$, $S^{(0)}_6$, and $S^{(1)}_1$ as well as the plate electric field $E^{(0)}_2$ and $E^{(1)}_1$ are related to the plate displacements and electric potential $\phi^{(1)}$ through[23,25]

$$\begin{aligned} &S^{(0)}_5 = u^{(0)}_{3,1}, \quad S^{(0)}_6 = u^{(0)}_{2,1} + u^{(1)}_1, \quad S^{(1)}_1 = u^{(1)}_{1,1}, \\ &E^{(0)}_2 = -\phi^{(1)}, \quad E^{(1)}_1 = -\phi^{(1)}_{,1}. \end{aligned} \tag{3}$$

The plate material constants in Eqs. (2) are defined by[23,25]

$$\gamma_{11} = s_{33}/(s_{11}s_{33} - s^2_{13}), \quad \psi_{11} = d_{11}\gamma_{11} + d_{13}\gamma_{13}, \tag{4}$$

where s_{pq} are the usual elastic compliance. d_{kp} are piezoelectric constants different from and related to e_{kp}. κ_1 in Eqs. (2) is a parameter called the shear correction factor, given by[23,25]

$$\kappa_1^2 = \frac{\pi^2}{12}\left(1 - \frac{8}{\pi^2}k^2_{26}\right), \; k^2_{26} = \frac{e^2_{26}}{\varepsilon_{22}\hat{c}_{66}}, \; \hat{c}_{66} = c_{66} + \frac{e^2_{26}}{\varepsilon_{22}}. \tag{5}$$

With successive substitutions from Eqs. (2) and (3), equation (1) can be written as three equations for $u^{(0)}_3$, $u^{(0)}_2$, and $u^{(1)}_1$ as follows:[23,25]

$$\kappa_1 c_{56}u^{(0)}_{2,11} + c_{55}u^{(0)}_{3,11} + \kappa_1 c_{56}u^{(1)}_{1,1} + e_{25}\phi^{(1)}_{,1} = \rho\ddot{u}^{(0)}_3, \tag{6a}$$

$$\kappa_1^2 c_{66}u^{(0)}_{2,11} + \kappa_1 c_{56}u^{(0)}_{3,11} + \kappa_1^2 c_{66}u^{(1)}_{1,1} + \kappa_1 e_{26}\phi^{(1)}_{,1} = \rho\ddot{u}^{(0)}_2, \tag{6b}$$

$$\gamma_{11}u^{(1)}_{1,11} + \psi_{11}\phi^{(1)}_{,11} - 3b^{-2}\left[\kappa_1 c_{56}u^{(0)}_{3,1} + \kappa_1^2 c_{66}(u^{(0)}_{2,1} + u^{(1)}_1) + \kappa_1 e_{26}\phi^{(1)}\right] = \rho\ddot{u}^{(1)}_1. \tag{6c}$$

For electrically forced vibrations of a fully electroded plate, $\phi^{(1)}$ is related to the driving voltage V across the plate thickness through[23,25]

$$\phi^{(1)} = \frac{1}{2b}V\exp(\mathrm{i}\omega t). \tag{7}$$

Therefore the spatial derivative of $\phi^{(1)}$ in Eqs. (6) vanishes. We note that equation (7) is for a plate driven by an electric field in the plate thickness direction or the so-called thickness field excitation (TFE). A plate can also be driven by an in-plane electric field or the so-called lateral field excitation (LFE).[26–28] We consider time-harmonic motions and use the usual complex notation. All fields have the same time dependence factor, which will be dropped in the following. The equations in Eqs. (6) are a system of ordinary differential equations with constant coefficients whose solution can be found in a standard manner. To calculate the charge on the electrodes, we need the following electric constitutive relation:[23,25]

$$D^{(0)}_2 = \int_{-b}^{b} D_2\,\mathrm{d}x_2 = 2b\left(e_{25}S^{(0)}_5 + \kappa_1 e_{26}S^{(0)}_6 + \varepsilon_{22}E^{(0)}_2\right). \tag{8}$$

The charge on and the current flowing into the top electrode of the resonator are[23,25]

$$Q_{\mathrm{e}} = -2c\int_{-a}^{a} D_2\,\mathrm{d}x_1, \quad I = \dot{Q}_{\mathrm{e}} = \mathrm{i}\omega Q_{\mathrm{e}}, \tag{9}$$

where

$$D_2 \cong \frac{D_2^{(0)}}{2b} = e_{25}u_{3,1}^{(0)} + \kappa_1 e_{26}(u_{2,1}^{(0)} + u_1^{(1)}) - \varepsilon_{22}\phi^{(1)}. \quad (10)$$

Then the frequency-dependent admittance of the resonator per unit plate area is given by[29]

$$Y = \frac{1}{4ac}\frac{I}{V}. \quad (11)$$

3. Pure thickness-shear vibration: $u_1^{(1)}$

For comparison, in this section, we consider the ideal case of a resonator vibrating in pure thickness-shear mode without coupling to flexure and face shear. Strictly speaking, pure thickness-shear vibration can only exist in infinite plates unbounded in the x_1 direction. For finite plates, when couplings to other modes are weak, the plates can be considered as vibrating in pure thickness-shear modes approximately. For pure thickness shear, from Eq. (6c), the boundary-value problem is

$$\gamma_{11}u_{1,11}^{(1)} + \psi_{11}\phi_{,11}^{(1)} - 3b^{-2}(\kappa_1^2 c_{66}u_1^{(1)} + \kappa_1 e_{26}\phi^{(1)}) = -\rho\omega^2 u_1^{(1)}, \quad |x_1| < a, \quad (12a)$$

$$T_{12}^{(0)} = 0, \quad x_1 = \pm a, \quad (12b)$$

where we have included free-edge boundary conditions. The general solution of the homogeneous form of Eq. (12a) with $\phi^{(1)} = 0$ symmetric in x_1 can be written as

$$u_1^{(1)h} = C\cos\xi x_1, \quad \xi = \sqrt{\frac{\rho\omega^2 - \frac{3}{b^2}\kappa_1^2 c_{66}}{\gamma_{11}}}, \quad (13)$$

where C is an undetermined constant. A particular solution of the inhomogeneous form of Eqs. (12a) can be found as

$$u_1^{(1)p} = \frac{3\kappa_1 e_{26}V}{2\gamma_{11}\xi^2 b^3}. \quad (14)$$

Then the general symmetric solution of the inhomogeneous form of Eqs. (12a) is

$$u_1^{(1)} = u_1^{(1)h} + u_1^{(1)p}. \quad (15)$$

Substitution of Eq. (15) into Eqs. (12b) determines C:

$$C = -\frac{e_{26}V}{2b\cos(\xi a)}\left(\frac{1}{\kappa_1 c_{66}} + \frac{3\kappa_1}{\gamma_{11}\xi^2 b^2}\right). \quad (16)$$

Then the admittance can be calculated using Eqs. (7)–(11). If $\cos\xi a$ in the denominator of Eq. (16) is set to zero, it determines the resonant frequencies of the resonator as

$$\xi a = a\sqrt{\frac{\rho\omega^2 - \frac{3}{b^2}\kappa_1^2 c_{66}}{\gamma_{11}}} = n\pi + \frac{\pi}{2}, \quad n = 0, 1, 2, \ldots. \quad (17)$$

As a numerical example, we consider a resonator of a typical thickness $2b = 0.4$ mm. An unbounded plate ($2a = \infty$) with this thickness has a fundamental thickness-shear frequency $\omega_0 = 2.599099 \times 10^7$ s^{-1}. To take material damping into consideration, in the numerical calculation, complex elastic stiffness $c_{pq}(1 + \mathrm{i}Q^{-1})$ and compliance $s_{pq}(1 - \mathrm{i}Q^{-1})$ are used where Q is a positive and large real number (material quality factor). $Q = 10^3$ is used in our calculation. This value is smaller than the usual material Q of quartz which is of the order of 10^5. $Q = 10^3$ is used so that resonances are not too sharp and narrow to be shown graphically. $Q = 10^3$ may be understood as a representation of the damping of the whole structure of the resonator including damping from the supports or mounting and air resistance, etc. Numerical results for resonant frequencies from Eq. (17) are presented in Fig. 2(a) versus the plate aspect ratio. For a given aspect ratio, there are many (infinite) resonant frequencies as shown in Eq. (17). Only three of them in the frequency range of interest are shown. The nearly flat one with ω/ω_0 slightly above one with $n = 0$ in Eq. (17) is the fundamental mode of main interest. Near this mode, the admittance with a unit of S=siemens=1/Ω assumes maxima as shown in Fig. 2(b).

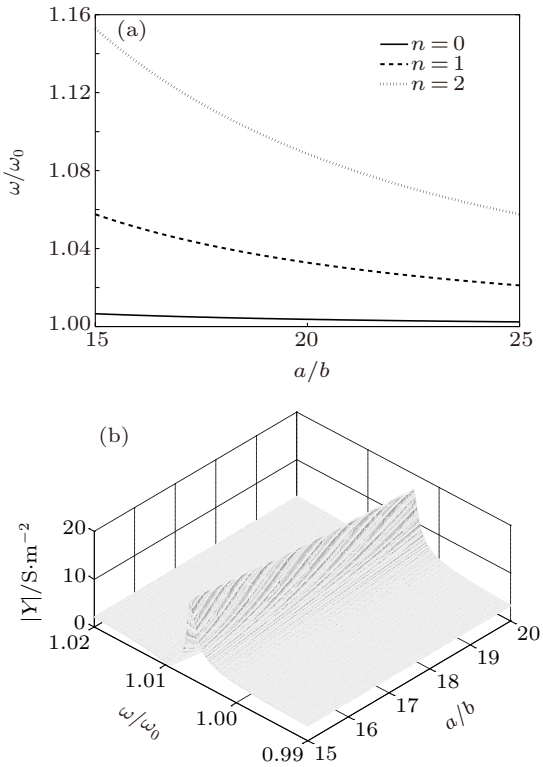


Fig. 2. The pure thickness shear: (a) frequency spectra and (b) admittance/m^2.

4. Coupled thickness-shear and flexure: $u_1^{(1)}$ and $u_2^{(0)}$

It can be seen from Eqs. (6) that, when the modes have x_1 dependence which is usually the case for finite plates, thickness shear $u_1^{(1)}$ and flexure $u_2^{(0)}$ are coupled. In this section we examine the effect of this coupling on admittance. From Eqs. (6b) and (6c), the boundary-value problem is:

$$\kappa_1^2 c_{66}u_{2,11}^{(0)} + \kappa_1^2 c_{66}u_{1,1}^{(1)} + \kappa_1 e_{26}\phi_{,1}^{(1)} = -\rho\omega^2 u_2^{(0)}, \quad |x_1| < a, \quad (18a)$$

$$\gamma_{11}u_{1,11}^{(1)} + \psi_{11}\phi_{,11}^{(1)} - 3b^{-2}[\kappa_1^2 c_{66}(u_{2,1}^{(0)} + u_1^{(1)}) + \kappa_1 e_{26}\phi^{(1)}] = -\rho\omega^2 u_1^{(1)}, \quad |x_1| < a, \quad (18b)$$

$$T_{12}^{(0)} = 0,\ T_{11}^{(1)} = 0,\ x_1 = \pm a. \tag{18c}$$

The general solution to Eq. (18a) with $u_1^{(1)}$ symmetric in x_1 can be written as

$$\begin{aligned} u_1^{(1)} &= A_1 \cos(\xi_1 x_1) + A_2 \cos(\xi_2 x_1) + \tilde{u}_1^{(1)}, \\ u_2^{(0)} &= B_1 \sin(\xi_1 x_1) + B_2 \sin(\xi_2 x_1), \end{aligned} \tag{19}$$

where

$$\tilde{u}_1^{(1)} = \frac{3e_{26}\kappa_1 V}{2b^3}\left(\rho\omega^2 - \frac{3}{b^2}\kappa_1^2 c_{66}\right)^{-1}. \tag{20}$$

ξ_1^2 and ξ_2^2 are the two roots of the following quadratic equation for ξ^2

$$\gamma_{11}\xi^4 - \rho\omega^2\left(\frac{\gamma_{11}}{c_{66}\kappa_1^2} + 1\right)\xi^2 + \rho\omega^2\left(\frac{3}{b^2} - \frac{\rho\omega^2}{c_{66}\kappa_1^2}\right) = 0. \tag{21}$$

A_1, A_2, B_1, and B_2 are undetermined constants. They are related by the following two relations:

$$B_m = \xi_m\left(\frac{\rho\omega^2}{\kappa_1^2 c_{66}} - \xi_m^2\right)^{-1} A_m, \quad m = 1, 2. \tag{22}$$

Therefore there are two independent undetermined constants. Substitution of Eq. (19) into the boundary conditions in Eq. (18c) determines A_1, A_2, B_1, and B_2. Then the admittance can be calculated using Eqs. (7)–(11). In the special case when the driving voltage $V = 0$, the free vibration solution is obtained which determines the resonant frequencies.

Figure 3(a) shows the free vibration frequencies of the modes of interest (corresponding to the modes with $n = 0$ in Eq. (17)) when ω/ω_0 is slightly larger than one. Comparison of Fig. 2(a) and Fig. 3(a) shows that, due to the coupling to flexure, the nearly flat curve with $n = 0$ in Fig. 2(a) breaks into sections by another family of curves related to flexure. Near the ends of each section, coupling to flexure is known to become severe and the corresponding values of a/b should be avoided in resonator design.[1] Figure 3(b) clearly shows that, near the ends of the flat sections in Fig. 3(a), when coupling to flexure is strong, the admittance drops significantly. Figure 3 represents the current understanding of the effect of mode coupling on admittance, except that we have plotted Fig. 3(b) more generally, using a surface. The results of Refs. [14] and [15] represent the intersection of the surface in Fig. 3(b) with a plane defined by a constant ω.

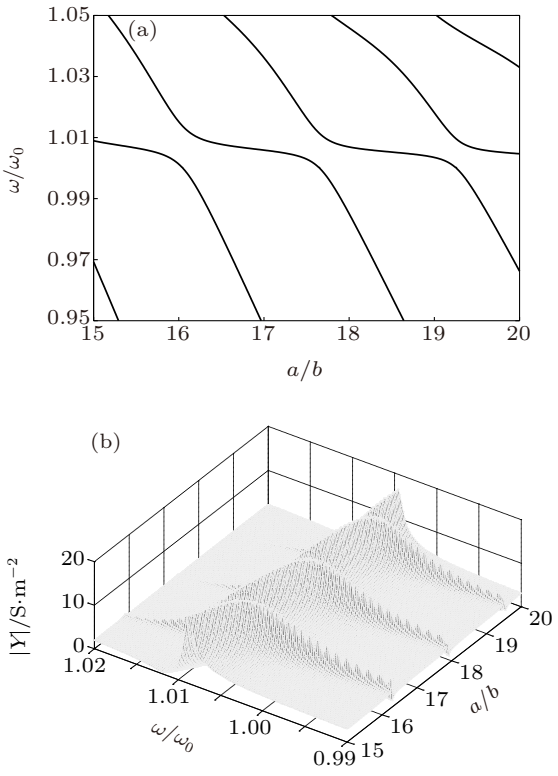


Fig. 3. Coupled thickness shear and flexure: (a) frequency spectra, (b) admittance/m^2.

5. Coupled thickness-shear, flexure, and face-shear: $u_1^{(1)}$, $u_2^{(0)}$, and $u_3^{(0)}$

From Eqs. (6), it can be seen that both the thickness-shear mode and the flexural mode are coupled to the face-shear mode through the elastic constant c_{56}. Since c_{56} is relatively small,[29] this coupling was rarely studied in frequency analysis. The effect of c_{56} on admittance is little known and will be examined below. The boundary-value problem is:

$$\kappa_1 c_{56} u_{2,11}^{(0)} + c_{55} u_{3,11}^{(0)} + \kappa_1 c_{56} u_{1,1}^{(1)} + e_{25}\phi_{,1}^{(1)} = -\rho\omega^2 u_3^{(0)},\ |x_1| < a, \tag{23a}$$

$$\kappa_1^2 c_{66} u_{2,11}^{(0)} + \kappa_1 c_{56} u_{3,11}^{(0)} + \kappa_1^2 c_{66} u_{1,1}^{(1)} + \kappa_1 e_{26}\phi_{,1}^{(1)} = -\rho\omega^2 u_2^{(0)},\ |x_1| < a, \tag{23b}$$

$$\gamma_{11} u_{1,11}^{(1)} + \psi_{11}\phi_{,11}^{(1)} - 3b^{-2}[\kappa_1 c_{56} u_{3,1}^{(0)} + \kappa_1^2 c_{66}(u_{2,1}^{(0)} + u_1^{(1)}) + \kappa_1 e_{26}\phi^{(1)}] = -\rho\omega^2 u_1^{(1)},\ |x_1| < a, \tag{23c}$$

$$T_{13}^{(0)} = 0, \quad T_{12}^{(0)} = 0, \quad T_{11}^{(1)} = 0, \quad x_1 = \pm a. \tag{23d}$$

Depending on the driving frequency, the general solution to Eqs. (23) with $u_1^{(1)}$ symmetric in x_1 can be written as

$$\begin{Bmatrix} u_1^{(1)} \\ u_2^{(0)} \\ u_3^{(0)} \end{Bmatrix} = \begin{Bmatrix} \sum_{m=1}^{3} A_m \cos(\xi_m x_1) + \tilde{u}_1^{(1)} \\ \sum_{m=1}^{3} B_m \sin(\xi_m x_1) \\ \sum_{m=1}^{3} C_m \sin(\xi_m x_1) \end{Bmatrix}, \quad \text{when} \quad \omega^2 > \frac{3\kappa_1^2 c_{66}}{\rho b^2}, \tag{24}$$

or

$$\begin{Bmatrix} u_1^{(1)} \\ u_2^{(0)} \\ u_3^{(0)} \end{Bmatrix} = \begin{Bmatrix} \sum_{m=1}^{2} A_m \cos(\xi_m x_1) \\ \sum_{m=1}^{2} B_m \sin(\xi_m x_1) \\ \sum_{m=1}^{2} C_m \sin(\xi_m x_1) \end{Bmatrix} + \begin{Bmatrix} A_3 \cosh(\xi_3 x_1) + \tilde{u}_1^{(1)} \\ B_3 \sinh(\xi_3 x_1) \\ C_3 \sinh(\xi_3 x_1) \end{Bmatrix}, \quad \text{when} \quad 0 < \omega^2 < \frac{3\kappa_1^2 c_{66}}{\rho b^2}, \tag{25}$$

where ξ_1^2, ξ_2^2, and ξ_3^2 are the three roots of the cubic equation for ξ^2 obtained by setting the coefficient matrix of the following linear homogeneous equations of A, B, and C to zero:

$$\begin{bmatrix} -\kappa_1 c_{56}\xi & -\kappa_1 c_{56}\xi^2 & \rho\omega^2 - c_{55}\xi^2 \\ -\kappa_1^2 c_{66}\xi & \rho\omega^2 - \kappa_1^2 c_{66}\xi^2 & -\kappa_1 c_{56}\xi^2 \\ \rho\omega^2 - \gamma_{11}\xi^2 - 3b^{-2}\kappa_1^2 c_{66} & -3b^{-2}\kappa_1^2 c_{66}\xi & -3b^{-2}\kappa_1 c_{56}\xi \end{bmatrix} \begin{Bmatrix} A \\ B \\ C \end{Bmatrix} = \begin{Bmatrix} 0 \\ 0 \\ 0 \end{Bmatrix}. \tag{26}$$

A_m, B_m, and C_m are undetermined constants. For each value of m, A_m, B_m, and C_m are proportional to an eigenvector of Eq. (26) and are thus related. There are three independent undetermined constants. Substitution of Eq. (24) or Eq. (25) into the boundary conditions in Eq. (23d) determines A_m, B_m, and C_m.

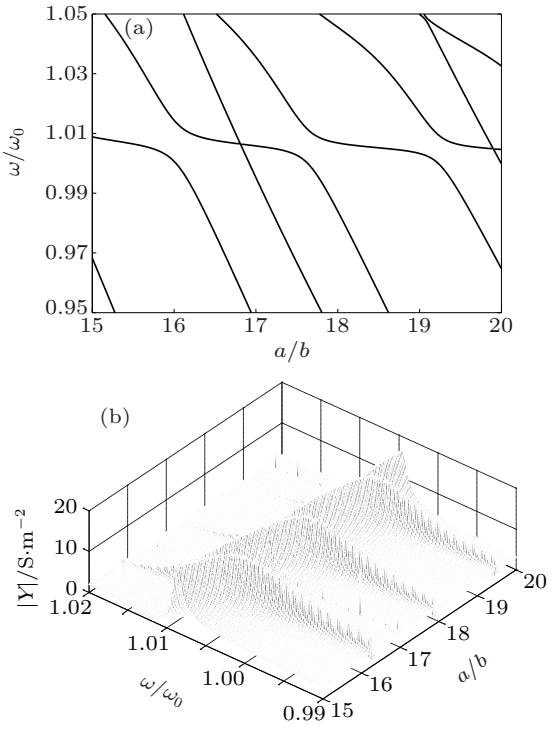


Fig. 4. Coupled thickness shear, flexure, and face shear: (a) frequency spectra, (b) admittance/m^2.

Figures 4(a) and 4(b) show the results from free and forced vibration analyses, respectively. Comparison of Fig. 3(a) with Fig. 4(a) shows that, due to the coupling to the face-shear mode, there are additional curves in the frequency spectra with what seem to be "intersections" with the nearly flat sections and the corresponding values of a/b may be undesirable in design. The admittance in Fig. 4(b) shows that along the curves related to the face shear in Fig. 4(a), the admittance has additional peaks or drops. These additional peaks and drops are small and sharp. The main problem is that they occur when the admittance is supposed to be smooth and the effect of flexure is already avoided, and therefore they require additional considerations in design. It should be noted that the coupling to the face-shear modes may have other undesirable implications. For example, the face-shear mode does not have a cutoff frequency[2,25] and the related energy trapping[2,25] behavior. As a consequence, the unwanted coupling to the face-shear mode may also cause energy leaking at the mounting points.

Figure 4 represents the main contribution of the present paper and deserves a closer look. In Fig. 5 we magnify the area near an "intersection" between thickness shear and face shear in Fig. 4(a). It can be seen that the "intersection" in Fig. 4(a) is not a real intersection. The two curves in fact turn away from each other just as a coupled theory typically predicts.

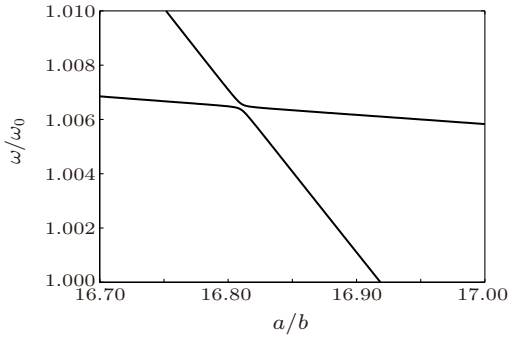


Fig. 5. Local view of the coupling between thickness shear and face shear.

The three-dimensional plot in Fig. 4(b) shows the overall behavior of the admittance clearly. However, for design, it is more convenient to have two-dimensional plots for admittance versus a/b[14,15] like what is shown in Fig. 6. The curves in Fig. 6 are intersections of the surface in Fig. 4(b) with planes of constant frequency. They are sensitive to the frequency. In addition to the major admittance drops related to the coupling with flexure, there are additional sharp peaks and drops due to the coupling with face shear. They occur in otherwise smooth portions of the curves.

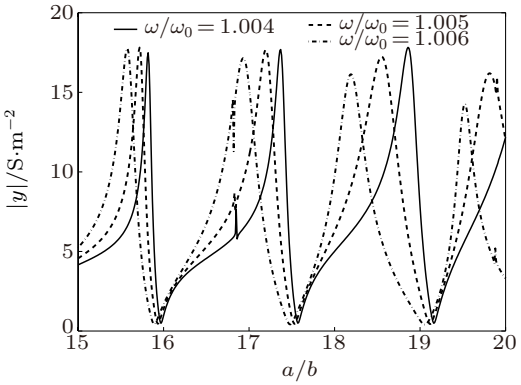


Fig. 6. Admittance/m^2 versus a/b for coupled thickness shear, flexure, and face shear.

6. Conclusion

Quartz thickness-shear resonator admittance with couplings to flexure and face shear is obtained from forced vibration analyses. Results show that at the fundamental thickness-shear mode, admittance assumes maxima. The coupling to flexure causes severe drops of admittance. Coupling to face shear results in additional, small, and sharp peaks or drops. These additional peaks or drops are within regions of the aspect ratio where the coupling to flexure is already avoided. Therefore they may affect the resonator performance in ways unexpected in current design practice. The coupling to face shear may also affect resonator performance in other ways because face shear does not have energy trapping. Therefore values of a/b corresponding to couplings to flexure and face shear should all be avoided in design in general.

References

[1] Mindlin R D 1951 *J. Appl. Phys.* **22** 316
[2] Mindlin R D and Lee P C Y 1966 *Int. J. Solids Structures* **2** 125
[3] Mindlin R D and Spencer W J 1967 *J. Acoust. Soc. Am.* **42** 1268
[4] Tiersten H F 1985 *J. Acoust. Soc. Am.* **78** 1684
[5] Yong Y K and Stewart J T 1991 *IEEE Trans. Ultrason., Ferroelect., Freq. Control* **38** 67
[6] Wang J and Zhao W H 2005 *IEEE Trans. Ultrason., Ferroelect., Freq. Control* **52** 2023
[7] Wang J N, Hu Y T and Yang J S 2010 *IEEE Trans. Ultrason., Ferroelect., Freq. Control* **57** 1146
[8] Chen G J, Wu R X, Wang J, Du J K and Yang J S 2012 *IEEE Trans. Ultrason., Ferroelect., Freq. Control* **59** 811
[9] Wang J and Yang J S 2000 *Appl. Mech. Rev.* **53** 87
[10] Mindlin R D 1952 *J. Appl. Phys.* **23** 83
[11] Tiersten H F and Mindlin R D 1962 *Quart. Appl. Math.* **20** 107
[12] Bleustein J L and Tiersten H F 1968 *J. Acoust. Soc. Am.* **43** 1311
[13] Mindlin R D 1974 *Int. J. Solids Structures* **10** 453
[14] Zhang W P 1998 *Proc. 1998 IEEE Int. Freq. Control Sym.* 981
[15] Zhang W P and Doyle M 2000 *Mechanics of Electromagnetic Materials and Structures,* ed. Yang J S and Maugin G A (Amsterdam: IOS) p. 147
[16] Lee P C Y and Wang J 1996 *J. Appl. Phys.* **79** 3411
[17] Lee P C Y and Lin W S 1998 *J. Appl. Phys.* **83** 7822
[18] Wang J, Yu J D, Yong Y K and Imai T 2000 *Int. J. Solids Structures* **37** 5653
[19] Wang J, Zhao W H and Du J K 2006 *Ultrasonics.* **44** 869
[20] Zhang C L, Chen W Q and Yang J S 2009 *Int. J. Appl. Elect. Mech.* **31** 207
[21] Yong Y K, Patel M S and Tanaka M 2010 *IEEE Trans. Ultrason., Ferroelect., Freq. Control* **57** 1831
[22] Mindlin R D 1961 *Quart. Appl. Math.* **19** 51
[23] Mindlin R D 1972 *Int. J. Solids Structures* **8** 895
[24] Lee P C Y, Syngellakis S and Hou J P 1987 *J. Appl. Phys.* **61** 1249
[25] Yang J S 2006 *The Mechanics of Piezoelectric Structures* (Singapore: World Scientific) Chap. 2 and Chap. 4
[26] Wang W Y, Zhang C, Zhang Z T, Liu Y and Feng G P 2009 *Chin. Phys. B* **18** 795
[27] Ma T F, Zhang C, Feng G P and Jiang X N 2010 *Chin. Phys. B* **19** 087701
[28] Ma T F, Zhang C, Jiang X N and Feng G P 2011 *Chin. Phys. B* **20** 057701
[29] Tiersten H F 1969 *Linear Piezoelectric Plate Vibrations* (New York: Plenum) p. 186